Journal of Materials Chemistry A

ROYAL SOCIETY OF CHEMISTRY

PAPER

View Article Online
View Journal

Cite this: DOI: 10.1039/d5ta09779g

Revealing the photochemical activity of fluorographene towards organic transformations: selective aerobic photooxidation of sulfides to sulfoxides

Alessandro Tabussi,[a] Stamatis K. Serviou,[a] Miroslav Medveď,[bc] Vítězslav Hrubý,[b] Juraj Filo,[d] Petr Lazar,[b] Marek Cigáň,[d] Demetrios D. Chronopoulos,[*a] Michal Otyepka[be] and Christoforos G. Kokotos[*a]

Received 29th November 2025
Accepted 6th February 2026

DOI: 10.1039/d5ta09779g

rsc.li/materials-a

Carbon-based materials have been widely applied as metal-free and effective photochemical promoters or catalysts for organic transformations, significantly advancing synthetic chemistry and enhancing the sustainability of the reactions. In this study, fluorographene (FG) was successfully employed as an efficient two-dimensional and non-metal photochemical promoter for the selective aerobic oxidation of sulfides to the corresponding sulfoxides in methanol under blue light at 456 nm and air as the oxidant. The application of the aforementioned protocol in a broad range of organic sulfides provided the corresponding sulfoxides in moderate to excellent yields. The catalytic mechanism was elucidated by the performance of several control experiments and theoretical calculations, confirming the predominant roles of singlet oxygen and superoxide anions for the successful oxidation of sulfides.

1 Introduction

Nowadays, organic synthetic photochemistry is recognized as an elegant and modern field, where unprecedented organic transformations are performed *via* the assistance of visible light.[1–4] The sustainability of photocatalysis can be further enhanced through the replacement of photocatalysts based on expensive metals (*e.g.*, Ru and Ir) by organic molecules[4–7] or non-metal nanomaterials.[8–12] In particular, heterogeneous metal-free photochemical promoters offer significant advantages, including high stability under reaction conditions, facile separation from the reaction system, and recyclability.[13–15] Due to their exceptional and tunable physicochemical and electronic properties, carbonaceous nanomaterials are prominent members among metal-free photocatalysts,[11] being employed either as pristine (*e.g.*, fullerenes)[16] or synthesized [*e.g.*, carbon nitrides (CNs) and carbon dots (CDs)][17–20] nano-photocatalysts or as supports [*e.g.*, carbon nanotubes (CNTs) and graphene] of photoactive organic molecules towards the preparation of hybrid photocatalysts with enhanced activity, due to synergy.[15,21]

Graphene is a photocatalytically inert material due to its zero-bandgap semimetallic nature. Hence, the extraordinary physicochemical, optical, electrical, and electronic properties of graphene have been exploited in photocatalysis through its hybridization with semiconductors, thereby improving their photocatalytic activities.[22] Owing to its photocatalytic inertness, graphene's utilization as a photochemical promoter for organic transformations has not been reported in literature yet, apart from a pioneer study, which presented the photochemical hydroacylation of dialkyl azodicarboxylates by graphite flakes (*i.e.*, precursor of graphene) under visible-light irradiation

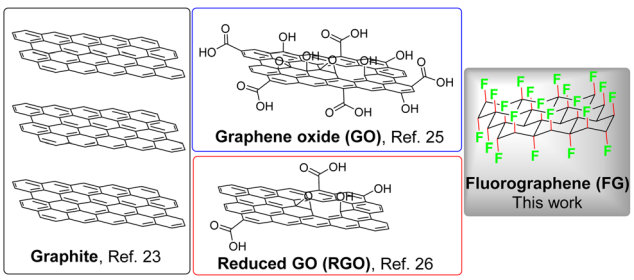

Scheme 1 Structures of the already employed graphene-based carbocatalysts as photochemical promoters for organic transformations.

[a]Laboratory of Organic Chemistry, Department of Chemistry, National and Kapodistrian University of Athens, Panepistimiopolis, Athens 15771, Greece. E-mail: ckokotos@chem.uoa.gr; dchrono@chem.uoa.gr

[b]Regional Centre of Advanced Technologies and Materials, Czech Advanced Technology and Research Institute (CATRIN), Palacký University Olomouc, Olomouc 779 00, Czech Republic

[c]Department of Chemistry, Faculty of Natural Sciences, Matej Bel University, Tajovského 40, 974 01 Banská Bystrica, Slovakia

[d]Department of Organic Chemistry, Faculty of Natural Sciences, Comenius University Bratislava, Ilkovičova 6, 842 15 Bratislava, Slovakia

[e]IT4Innovations, VŠB – Technical University of Ostrava, Ostrava-Poruba 708 00, Czech Republic

(Scheme 1).[23] As the chemical modification of graphene has been applied as an effective method for the concurrent preparation of graphene-based materials with open bandgap and high dispersibility,[22,24] graphene oxide (GO) and reduced GO (rGO), the most common graphene derivatives, have been utilized as photochemical carbocatalysts for the performance of organic transformations (Scheme 1).[25,26] However, the broad applicability of these materials is hindered by significant drawbacks, such as the harsh and non-controllable conditions required for the synthesis of GO, which are then reflected in high chemical and structural complexity of GO.

Fluorination of graphene, namely the conversion of the sp^2-hybridized carbons of graphene to C–F sp^3 bonds, is a chemical approach that leads to the synthesis of fluorographene (FG, Scheme 1), a fully fluorinated counterpart of graphene.[27,28] FG can also be easily obtained *via* liquid phase exfoliation of commercial bulk graphite fluoride (GrF), which is a market-available material used as an industrial lubricant or electrode material.[29,30] FG has attracted significant interest due to its unique chemical reactivity, making it a valuable precursor for the synthesis of a wide portfolio of well-defined graphene derivatives.[30–34] At the BSE/GW_0@PBE level of theory, which combines accurate quasiparticle gaps with explicitly treated electron–hole interactions, the optical bandgap of FG was predicted to be 5.7 eV.[35] The onset of optical absorption was observed experimentally at 5.75 eV in accordance with the theoretical result.[35] Earlier observations of light emission[36] and absorption[37] of FG at around 3.5 eV have been ascribed to defects present within the real FG samples. Specifically, radical point defects induce midgap states into the electronic structure of FG, with the lowest transition at 3.1 eV.[35] Despite these defect-related features, bathochromic solvatochromism of carbon monofluoride (CF; bulk FG) has been observed by Watanabe *et al.*[38] In that study, dispersions of CF in various solvents appeared slightly darker. The measured emission spectra of CF in both non-polar (paraffin) and polar media (MeOH) exhibited emission maxima centred at approximately 460 nm (2.7 eV).

The selective oxidation of organic sulfides to the corresponding sulfoxides is a valuable transformation in organic synthesis,[39–44] since many sulfoxide-containing compounds are high-value-added chemical products, widely used in the pharmaceutical industry.[45] The exploitation of photochemistry towards this end provides remarkable advantages, such as the chemoselective oxidation to sulfoxides without the formation of sulfones as byproducts and the utilization of molecular oxygen as the oxidizing agent, in contrast to the conventional oxidation protocols.[44,46–49] In this context, metal-free carbon-based nanomaterials (*e.g.*, fullerenes, CDs, CNs, and CNT-based nanomaterials) have been utilized for this purpose.[50–57] However, the broad applicability of carbon-based nanomaterials in such photochemical organic reactions is prevented by critical challenges, such as the high cost of fullerenes (*i.e.*, C_{60} and C_{70}), the synthetic effort for functionalizing carbon allotropes and immobilizing photoactive units, harsh conditions, and lack of reproducibility for their fabrication.

Focusing on the already developed metal-free carbon-based photocatalysts, metal-free CN-based photocatalysts (Scheme 2-i) were synthesized by polymerizing organic compounds at high temperatures (>550 °C).[50–52] Furthermore, CNs in the synthesized bulk form exhibited low conversion and/or moderate selectivity in the photooxidation of sulfides to the corresponding sulfoxides, requiring either the use of excessive amounts of additives (*i.e.*, aldehydes) along with the catalyst[50] or the application of post-acidic[51] and/or thermal[52] treatment for achieving high photochemical performances. Importantly, in the case of using oxidized CNs as photocatalysts, the reactions were irradiated with a xenon lamp, a critical drawback of the applied protocol due to the xenon lamp's high energy consumption.[51] Moreover, the synthesis of CNs under harsh conditions remains a significant drawback for preparing CN-based hybrids, such as the CN/C_{60} photocatalyst (Scheme 2-ii).[53] Additionally, the high cost of C_{60} and the utilization of CN/C_{60} in high amounts further minimize the application of such a photocatalyst. To overcome this crucial issue, the use of fullerene soot, as an alternative and cheaper option to C_{60} or C_{70}, was proposed (Scheme 2-iii).[54] However, the scope of this method was limited to oxidizing dialkyl sulfides, following a singlet oxygen mechanism, whereas the expansion of the scope to aryl–alkyl sulfides (*e.g.*, thioanisole) was accomplished by the addition of triethylamine as the mediator of an electron

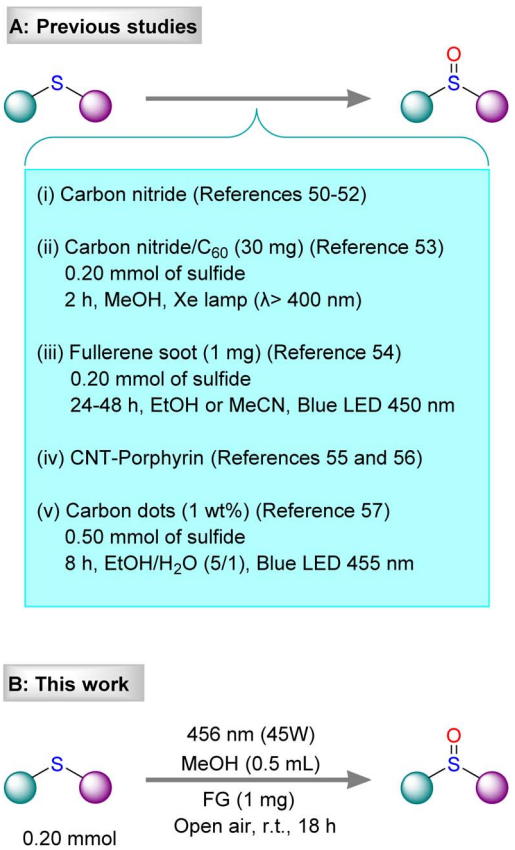

Scheme 2 Methods for the photooxidation of organic sulfides using metal-free carbon-based nanomaterials as photochemical promoters.

transfer mechanism. Moreover, fullerene soot is a non-well-defined raw material, as it is produced by vaporizing pure carbon in an inert atmosphere. Concerning the exploitation of carbon allotrope nanostructures as platforms for carrying photoorganocatalysts, porphyrin derivatives have been covalently or noncovalently immobilized onto CNTs (Scheme 2-iv).[55,56] Despite the high performance of these hybrid photocatalysts in the oxidation of sulfides under irradiation by a white LED lamp or sunlight, the high price and low photostability of porphyrins, along with the synthetic effort required for their loading onto modified CNTs, are significant drawbacks to the broad applicability of the as-prepared hybrid photocatalysts. Recently, CDs were successfully used to effectively oxidize sulfides to the corresponding sulfoxides.[57] However, as in the case of CNs synthesis, CDs are prepared under harsh conditions, which hamper their accurate reproducibility. In particular, in the reported study, the use of *N*,*N*-dimethylformamide (DMF) as the solvent and NH_4F as the additive (which effectively enhances the photochemical activity of the formed CDs) in the synthetic process, along with the lack of recyclability, are crucial handicaps of this method.[57] Therefore, the use of low-cost and easily accessible carbon-based photochemical promoters for the selective oxidation of sulfides to sulfoxides under environmentally friendly and specific irradiation wavelengths is an interesting field for research.

In this study, the use of FG as a metal-free photochemical promoter for organic transformations is reported for the first time. Developing an effective, mild, and sustainable protocol employing FG as the photochemical promoter, the chemoselective photooxidation of a plethora of organic sulfides to the corresponding sulfoxides was achieved in moderate to high yields, ranging from 32–97%. Control experiments demonstrated that among the various carbon materials, only the pristine FG exhibited sufficient photochemical activity. The low elimination of fluorine atoms from FG during the photochemical process resulted in the photocatalytic reduction of FG, thus preventing its recyclability. Finally, mechanistic studies involving several trapping experiments demonstrated that the photooxidation of sulfides proceeds through electron and/or energy transfer mechanisms, whereas theoretical calculations provided insight into the effectiveness of FG.

2 Results and discussion

Visible light-mediated aerobic oxidation of organic sulfides towards sulfoxides was chosen as the model reaction to probe the photocatalytic activity of FG in organic transformations.[44] Initially, crucial parameters for investigating the photochemical activity of FG were set. In this context, commercial GrF from Sigma-Aldrich was selected as the parent material for obtaining FG in suspension after 30 min sonication in acetonitrile, a common solvent in photochemistry. Due to the reported FG-solvent absorption maxima at 460 nm,[38] LED 456 nm was selected for irradiating the reaction in an open-air atmosphere at room temperature for 18 hours (Table 1). Notably, sulfide oxidation under LED 456 nm irradiation is negligible, as previous studies have demonstrated,[58] and that was confirmed by the performance of a control experiment in the absence of FG (Table 1, entry 1). Then, the conditions above were applied in the photooxidation of thioanisole (**1a**), and a moderate conversion (33%) of the desired sulfoxide **2a** was observed (Table 1, entries 2 and 4), thus demonstrating the activity of FG as a potential photosensitizer for generating reactive oxygen species (ROS). This finding was further confirmed by a control experiment, which showed that photooxidation did not proceed without irradiation (Table 1, entry 3). Additionally, a series of reactions employing other carbon allotrope nanostructures (*i.e.*, graphene or CNTs) as photocatalysts, instead of FG, indicated the photochemical inertness of graphene and CNTs for the performance of the photooxidation of **1a** (Table 1, entries 5–7), thus validating even further the photochemical activity of FG. Interestingly, the photochemical activity of cyanographene (GCN), a fluorine-free graphene derivative synthesized by using FG as precursor, was negligible (Table 1, entry 8), indicating that the photochemical activity of FG originates from the intact two-dimensional C–F network.

Having demonstrated the ability of FG to act as a photochemical promoter in the photooxidation of thioanisole (**1a**) to the corresponding sulfoxide **2a**, our efforts focused on the optimization of the reaction conditions. Solvent optimization revealed methanol as the most effective solvent for our photocatalytic system (Table S2, entry 2), which is consistent with other similar studies,[58] as MeOH plays a crucial role in selectivity during photooxidation due to its protic nature.

Table 1 Revealing the photochemical activity of FG in the photooxidation of thioanisole (**1a**) towards the corresponding sulfoxide **2a**[a]

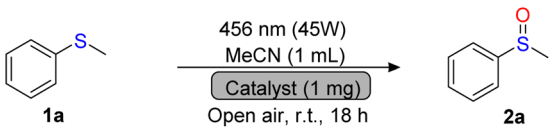

1a **2a**

Entry	Catalyst	Conversion (%)
1[b]	—	7
2	FG	33
3[c]	FG	—
4[d]	FG	35
5	Graphene	—
6	SWCNTs	3
7	MWCNTs	5
8	GCN	4

[a] The reaction was performed with thioanisole (**1a**) (25 mg, 0.20 mmol), catalyst (1 mg) in MeCN (1 mL), under Blue LED irradiation (Kessil PR160L, 456 nm). FG was obtained after 30 minutes of sonication of GrF (1 mg) in the reaction's solvent, before the addition of **1a**. The rest of the materials were sonicated for 30 minutes in the reaction's solvent, before the addition of **1a**. Conversion was determined by ^{1}H-NMR. [b] The reaction was performed in the absence of a photocatalyst. [c] The reaction was performed without irradiation. [d] The reaction was performed using 2 mg of GrF for producing FG. Graphene powder, single-walled (SW)CNTs, and multi-walled (MW)CNTs were purchased from Nanostructured & Amorphous Materials Inc. Cyanographene (GCN) was synthesized according to the reported procedure.[32]

Importantly, the high conversion of thioanisole (**1a**) to the corresponding sulfoxide **2a** by using the green solvent cyrene highlighted the ability of FG to be applied in an environmentally friendly photochemical system (Table S2, entry 10). The latter finding is very important, as water (the greenest solvent) cannot be used in protocols based on FG (Table S2, entry 8), due to its extremely high hydrophobicity.

A thorough investigation was then conducted to examine the influence of the wavelength of the irradiation sources on the reaction. According to the obtained results, the utilization of LED at 456 nm exhibited the highest performance for the photooxidation of **1a** (Table 2, entry 2). In comparison, LEDs utilizing irradiation wavelengths at 440 or 467 nm also displayed high reaction conversions (Table 2, entries 3 and 4). On the other hand, irradiation of the reaction under an LED at 525 nm or a compact fluorescent lamp (CFL) provided moderate or low conversions (Table S3, entries 4 and 5), respectively. The results are in good agreement with the UV-Vis spectrum of FG in MeOH, as the absorption maxima were centered at around 460 nm (Fig. S1). This absorption peak was absent in the UV-Vis spectrum of FG in MeCN, explaining the low conversion rates in MeCN solvent. These findings confirmed a correlation between the spectral regions where FG-solvent systems absorb and the effectiveness of FG's photochemical activity.

Afterward, our studies focused on determining the catalyst loading in the reaction mixture. In recent work related to conventional carbocatalysis, studies have shown that the surface of a carbocatalyst can become oversaturated, due to the dispersion of a high amount of it in a low volume of solvent, thereby rendering a significant portion of the carbocatalyst catalytically useless.[59] Taking this into account, along with the initial studies for probing the photochemical activity of FG, where the reaction conversion was similar for using 1 or 2 mg of FG dispersed in 1 mL of MeCN (Table 1, entries 2 and 4), the optimization of the catalyst loading in MeOH (the best solvent for our system, see Table S2) was carried out as well (Table 3). The reaction conversion was found to be similarly high in all cases, as the synthesis of sulfoxide **2a**, based on its isolation by column chromatography, was quantitative in 1/0.5 and 2/1.0 FG/MeOH (mg mL^{-1}) systems. Considering atom economy, a basic principle of Green Chemistry, the system 1 mg of FG and 0.5 mL of MeOH was chosen as the optimum. Next, monitoring the reaction by TLC showed that the full photooxidation of thioanisole (**1a**) is a relatively slow process, requiring approximately 18 h. According to the overall photocatalytic results by the optimization, the photooxidation of thioanisole (**1a**, 0.20 mmol) to the corresponding sulfoxide **2a** exhibited the best conversion (100%) and an excellent yield (92%) employing 1 mg of FG dispersed in 0.5 mL MeOH, LED 456 nm as the irradiation source, atmosphere oxygen as the solo oxidant and 18 h reaction time (Table 3, entry 2).

Having specified the optimum reaction conditions, we studied the scope of the photooxidation of organic sulfides (Scheme 3). Initially, the reaction was performed using phenyl–alkyl sulfides, namely compounds bearing a phenyl and alkyl group directly connected to sulfur (Scheme 3A). According to the catalytic results, the applied protocol in the photooxidation of sulfides **1a–d** afforded the corresponding sulfoxides in excellent yields (**2a–d**), regardless of the length or the structure of the alkyl moieties. Then, the study of the scope of the aforementioned type of thioethers was focused on those containing functionalities in the aliphatic chain (Scheme 3A). The results demonstrated the synthesis of sulfoxides in moderate yields (**2e–i**), with the exception of sulfoxide **2g**, which bears a hydroxyl group and achieved an excellent yield. Notably, the photooxidation of sulfide **1i** was performed in MeCN due to the obstacle of concurrent esterification in MeOH, which would also occur during oxidation. Afterward, our protocol was applied to alkyl–alkyl sulfides (Scheme 3B). The photooxidation of sulfides **1j–n** resulted in the formation of the corresponding

Table 2 Solvent and lamp optimization for the photooxidation of thioanisole (**1a**) to sulfoxide **2a**, using FG as a photochemical promoter[a]

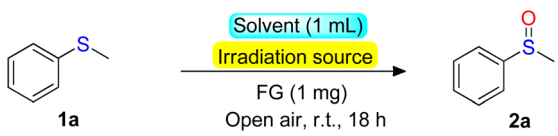

Entry	Solvent	Irradiation source (nm)	Conversion (%)
1	MeCN	456 nm	33
2	MeOH	456 nm	96 (75)
3	MeOH	440 nm	75
4	MeOH	467 nm	73

[a] The reaction was performed with thioanisole (**1a**) (25 mg, 0.20 mmol), FG (1 mg) in solvent (1 mL), under irradiation. FG was obtained after 30 minutes of sonication of GrF (1 mg) in the reaction's solvent, before the addition of **1a**. Conversion was determined by ^{1}H-NMR. Yield of **2a** after isolation by column chromatography is shown in parentheses.

Table 3 Optimization of the ratio FG/MeOH for the photooxidation of thioanisole (**1a**) to sulfoxide **2a**, using FG as a photochemical promoter[a]

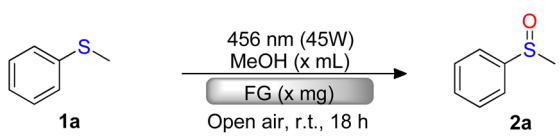

Entry	mg of FG/mL of MeOH	Conversion (%)
1	1 mg/1.0 mL	96 (75)
2	1 mg/0.5 mL	100 (92)
3	1 mg/2.0 mL	98 (79)
4	2 mg/1.0 mL	99 (95)

[a] The reaction was performed with thioanisole (**1a**) (25 mg, 0.20 mmol), employing the above-mentioned ratio of FG/MeOH, under blue LED irradiation (Kessil PR160L, 456 nm). FG was obtained after 30 minutes of sonication of GrF (1 mg) in the reaction's solvent, before the addition of **1a**. Conversion was determined by ^{1}H-NMR. Yield of **2a** after isolation by column chromatography is shown in parentheses.

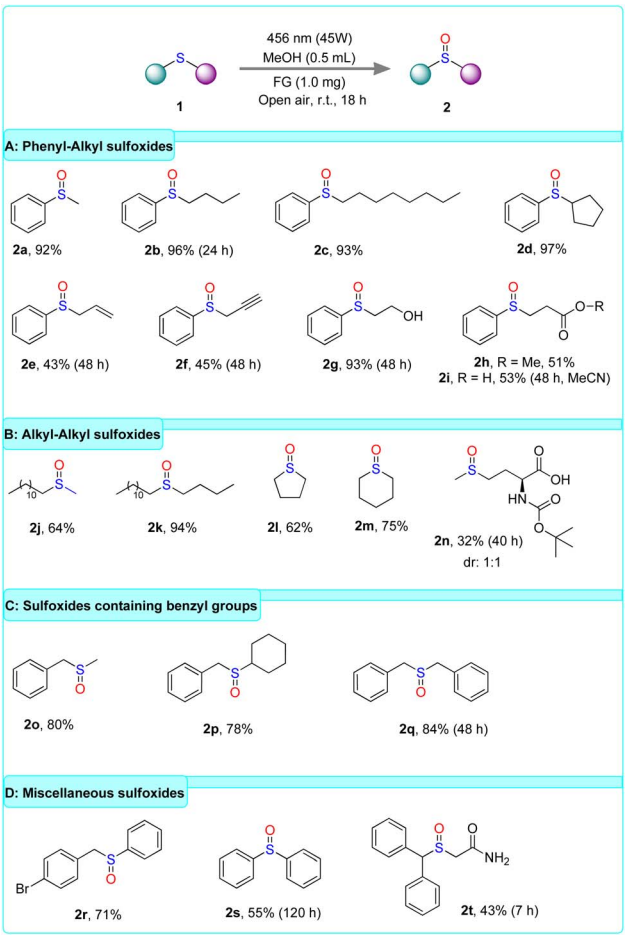

Scheme 3 Substrate scope of organic sulfides. Reported yields refer to yields after isolation by column chromatography.

sulfoxides in moderate to high yields for aliphatic or cyclic alkanes (**2j–m**). In contrast, synthesis of **2n** was afforded in low yield (32%). Next, the scope of benzyl–alkyl sulfides was also investigated (Scheme 3C). The photooxidation of sulfides bearing a benzyl group and an alkyl group (**1o–p**) afforded the corresponding sulfoxides in good yields (**2o–p**). Additionally, the oxidation of the symmetrical sulfide **1q**, where sulfur is linked with two benzyl groups, exhibited a high yield formation of sulfoxide **2q** (84%). Finally, the photooxidation of sulfides, which is not classified in the categories above, was also evaluated (Scheme 3D). In this context, sulfide **1r** containing benzyl–phenyl moieties was converted to the corresponding sulfoxide **2r** in good yield (71%). Importantly, our protocol was also effective for the oxidation of the symmetrical aryl–aryl sulfide **1s**, affording the corresponding sulfoxide **2s** in moderate yield (55%). Since the oxidation of diaryl sulfides occurs *via* an electron transfer event, the latter result indicates the mechanistic pathway following our developed protocol. Considering the presence of the sulfoxide moiety in several pharmaceutical active ingredients, our protocol was applied to the synthesis of modafinil (**2t**), a synthetic medicinal drug featuring a sulfoxide group.[60] After the synthesis of the sulfide **1t**, the photooxidation process was applied for 7 hours, providing the desired sulfoxide **2t** in 43%, employing a carbon-based metal-free photocatalyst for the first time. The irradiation time was set to 7 hours to prevent C–S fragmentation of the starting material or the product, due to the presence of a-benzylic hydrogen, which can occur with prolonged irradiation times.

To gain insight into the photochemical oxidation mechanism, several control experiments were conducted using the aforementioned optimized protocol. Initially, a significant reduction in the reaction conversion was observed when GrF was employed without sonication (Table 4, entry 1), indicating that the exfoliated FG layers of bulk GrF participate as the photocatalyst for effective photooxidation. Prolonged sonication (*i.e.*, 1 h) did not improve the photooxidation of thioanisole (**1a**), indicating that the system 1/0.5 FG/MeOH (mg mL^{-1}) was probably saturated, as no additional exfoliation of FG layers occurred.

Transmission electron microscopy (TEM) and atomic force microscopy (AFM) demonstrated the effective exfoliation of FG layers *via* the performance 30 min of sonication of GrF in 0.5 mL of MeOH (Fig. 1). AFM imaging (Fig. 1A) proved the presence of exfoliated sheets of with height as low as 2 nm (Fig. 1B) corresponding roughly to four FG layers.[30] TEM images showed transparent sheets as well (Fig. 1C) and indicated the sample's defective nature, as evidenced by wrinkles at the edges of the sheets (Fig. 1D).

Regarding the effectiveness of light in the reaction, the catalytic results revealed its necessity for photooxidation to proceed (Table 4, entry 2). In contrast, the absence of FG (*i.e.*, photocatalyst) or air (*i.e.*, oxygen) resulted in a low yield of **2a** (Table 4, entries 3 and 4), respectively, demonstrating the key roles of FG and oxygen in the photocatalytic oxidation system. Notably, photooxidation did not proceed under heating at 60 °C, indicating that the energy provided by the LED for the reaction's performance is light, not heat (Table 4, entry 5).

Table 4 Investigating the influence of each of the standard parameters for the photooxidation of thioanisole (**1a**) to sulfoxide **2a**, using FG as a photochemical promoter[a]

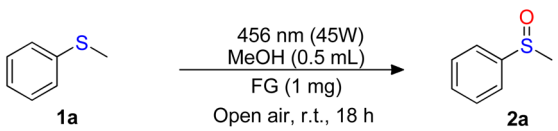

Entry	Deviation from standard conditions	Conversion (%)
1	No sonication	27
2	No irradiation	—
3	No catalyst	14
4	Argon atmosphere	14
5	Dark, 60 °C	3

[a] The reaction was performed with thioanisole (**1a**) (25 mg, 0.20 mmol), FG (1 mg) in solvent MeOH (0.5 mL) under blue LED irradiation (Kessil PR160L, 456 nm). FG was obtained after 30 minutes of sonication of GrF (1 mg) in the reaction's solvent, before the addition of **1a**. Conversion was determined by ^{1}H-NMR.

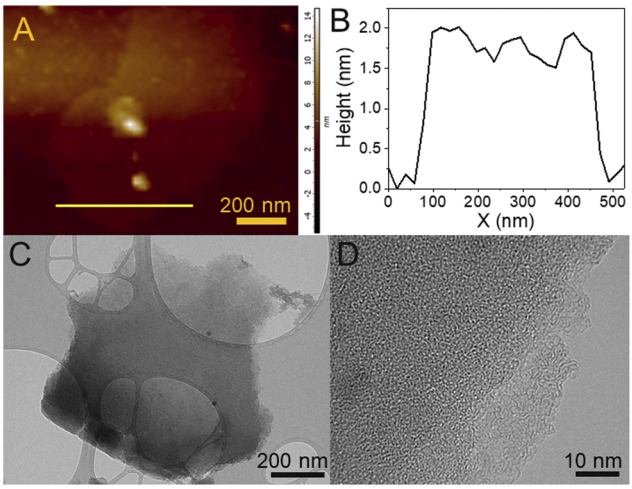

Fig. 1 Panel (A) shows an AFM image of the dry contents of FG sonicated in MeOH for 30 minutes, with the indicated path of the height profile shown in panel (B). Panels (C) and (D) show TEM images of the same sample of sonicated FG.

Afterward, a series of trapping experiments employing various quenchers was conducted to identify reactive species participating in the photooxidation of sulfides (Fig. 2). The photochemical transformation was significantly suppressed by adding a radical quencher [*i.e.*, 1,4-dimethoxybenzene, hydroquinone, or butylated hydroxytoluene (BHT)], conversion was also decreased if $CuSO_4$, acting as an electron quencher, was employed. Notably, using KI as a hole quencher led to an even larger reduction in the photooxidation efficiency, further hinting that the reaction is facilitated by demonstrating a crucial role of radicals in the reaction. The photogenerated electron–hole separation. In accordance with these results, the conversion was strongly suppressed by employing NaN_3 or 4-

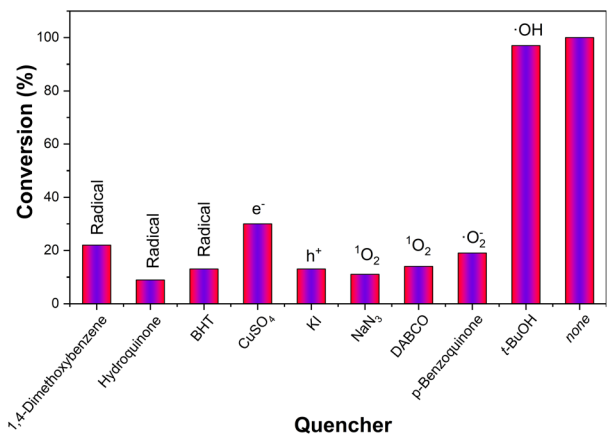

Fig. 2 The effect of quenchers on the photooxidation of thioanisole (**1a**) to sulfoxide **2a**, using FG as a photochemical promoter. The reaction was performed with thioanisole (**1a**) (25 mg, 0.20 mmol), FG (1 mg) in MeOH (0.5 mL), under Blue LED irradiation (Kessil PR160L, 456 nm). FG was obtained after 30 minutes of sonication of GrF (1 mg) in the reaction's solvent, before the addition of **1a** and quencher. Conversion was determined by ^{1}H-NMR.

diazabicyclo[2.2.2]octane (DABCO) as singlet oxygen ($^1O_2$) scavengers or *p*-benzoquinone as superoxide radical anion ($^{\bullet}O_2^-$) scavenger, thus indicating the involvement of ROS in the photooxidation of thioethers. On the other hand, the addition of *t*-BuOH as a hydroxyl radical quencher ($^{\bullet}$OH) did not influence the reaction, excluding the $^{\bullet}$OH formation during the photooxidation. In addition, the possibility of *in situ*-generated H_2O_2 acting as the oxidant for the photooxidation of organic sulfides was excluded by the iodometric method (Fig. S2–S4). Based on the trapping experiments, two mechanisms of the photooxidation of sulfides to the corresponding sulfoxides through the photochemical activity of FG can be proposed (Fig. 3). On the one hand, the photoinduced electron–hole separation, along with the sensitivity of the conversion to the presence of superoxide radical anions, suggests a concerted single-electron transfer (SET) mechanism (Fig. 3, right). The holes initiate sulfide oxidation to the corresponding radical cation (**II**), which subsequently reacts with the superoxide formed *via* oxygen reduction at the electron-rich sites. The formed dipolar peroxysulfoxide intermediate (**III**) reacts with another sulfide molecule, yielding the corresponding sulfoxide (**IV**). On the other hand, the strong inhibitory activity of singlet oxygen scavengers suggests an alternative energy transfer pathway (Fig. 3, left). Here, the generated singlet oxygen acts as an oxidation agent for sulfides also leading to the peroxysulfoxide intermediate (**III**), which yields the desired sulfoxide (**IV**) by reaction with another sulfide molecule.

The photogeneration of $^1O_2$ *via* irradiating the FG dispersions (in the absence of sulfides) using a 470 nm LED light source was also confirmed by independent experiments using 1,3-diphenylisobenzofuran (DPIBF) as a selective probe for singlet oxygen (Fig. S5). Importantly, the FG dispersion in MeOH exhibited significantly higher capacity to produce $^1O_2$ compared to the FG dispersion in MeCN, in line with a much less efficient photooxidation of sulfides in the latter solvent (Table S2). Eventually, the two mechanisms can take place simultaneously or can be linked *via* interconversion of $^1O_2$ and $^{\bullet}O_2^-$ species.

To assess the catalyst's stability and heterogeneity, a leaching test was performed (see SI). In this frame, FG was removed from the reaction mixture by filtration after 2 h of irradiation, and the reaction was allowed to proceed for an additional 16 h. The conversion of the photooxidation at 2 h (*i.e.*, 23%) did not increase after the catalyst's removal, confirming that FG was responsible for the photochemical activity observed, as no leaching of any photochemically active species in the reaction mixture occurred.

FG was recovered after the first cycle of the reaction *via* centrifugation to test its recyclability in the second photocatalytic run. Recovered FG (denoted as r-FG) was subjected to a new photocatalytic cycle, affording the desired sulfoxide **2a** in low yield (26%) after 18 h of irradiation. Interestingly, unlike gray pristine FG, the recovered precipitate r-FG was almost black after the reaction (Fig. S6), indicating the removal of fluorine atoms from FG's lattice. Owing to this latter observation, our study focused on characterizing r-FG using spectroscopic techniques. In contrast to the exfoliated FG, the FTIR

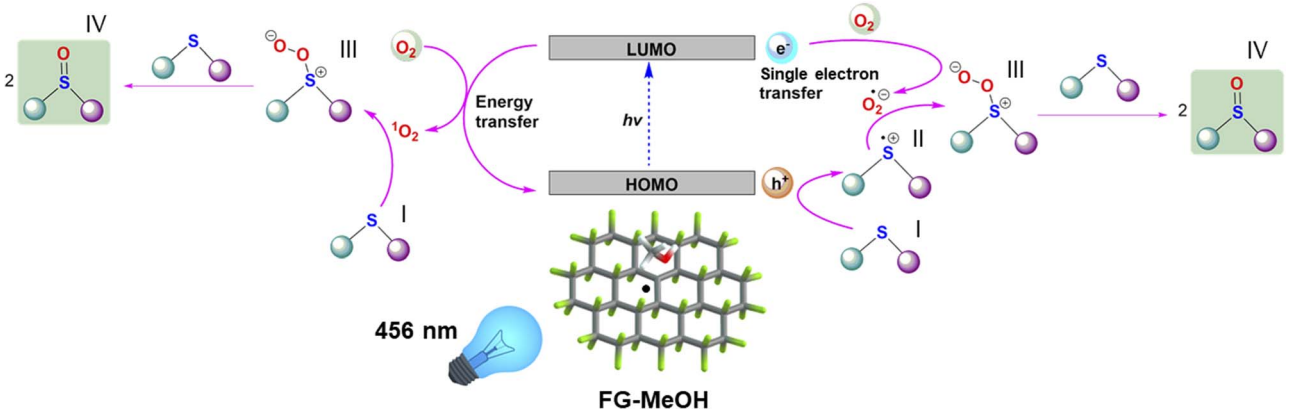

Fig. 3 Proposed mechanisms for the photooxidation of organic sulfides to the corresponding sulfoxides, using FG as a photochemical promoter.

spectrum of r-FG exhibited a small band at 1592 cm^{-1}, which is ascribed to the formation of C=C bonds, due to the elimination of a few fluorine atoms by the FG lattice (Fig. S7). Considering that ultraviolet irradiation of FG results in the elimination of fluorine atoms,[61] a control experiment was conducted by following our developed protocol without the addition of **1a** to study the effect of LED 456 nm on the FG structure. The FTIR spectrum of the formed material (denoted as *hν*-FG) demonstrated that the illumination was the reason for the low defluorination of FG, as a similar spectrum shape to the material r-FG was recorded (Fig. S7). In agreement with the latter data, a low reduction of fluorine atoms of r-FG and *hν*-FG with respect to the exfoliated FG by MeOH was recorded by X-ray photoelectron spectroscopy (XPS). Additionally, the F/C atomic ratios were calculated as 1.23, 0.87, and 0.87 for exfoliated FG, r-FG, and *hν*-FG, respectively (Fig. 4A–C), thus further corroborating the defluorination effect of LED 456 nm in FG. Finally, the deconvoluted C 1s XPS spectra of FG, r-FG, and *hν*-FG verified the defluorination of FG by the irradiation, since a band at 284.7 eV in the spectra of r-FG and *hν*-FG appeared, ascribed to the sp^2 carbons, which were formed as a result of defluorination (Fig. 4D–F). In particular, apart from the main C–F spectral line, the most prominent feature in the irradiated samples appeared at 285.7 eV, which corresponded to sp^2 carbons of C_4F-like motifs (C–C*–F and C*–C–F components).[62] The establishment of the extended sp^2 carbon network was evident through the appearance of components at 284.6 eV and 286.9 eV. The latter feature corresponds to sp^2 carbons with adsorbed fluoride anions.[62] Notably, the photolysis of FG has already been observed by Watanabe *et al.* in their study of CF.[38] They observed defluorination of CF upon prolonged irradiation of CF dispersions in alcohols, and concluded that formation of corresponding aldehydes, along with hydrogen fluoride, occurs. The longer the irradiation was, the lower the fluorine content was found.[38] Notably, the UV-Vis spectra of both materials r-FG and *hν*-FG did not display the peak centered at 460 nm, as it appeared at the spectrum of FG (Fig. S1).

Then, we focused our studies on rationalizing and overcoming the significant catalytic reduction of r-FG in the recycling process. The considerable decrease in the conversion could be ascribed either to the formed dark suspension of the system's second cycle, which hinders light penetration into the interior of the system, or to the alteration of the photochemical properties of the as-formed r-FG, in comparison with those of pristine FG. Based on the former speculation, a new photocatalytic run was conducted, employing the appropriate amount of FG with the addition of some drops of r-FG in MeOH (~0.5 mg of r-FG), to make the suspension dark. The conversion

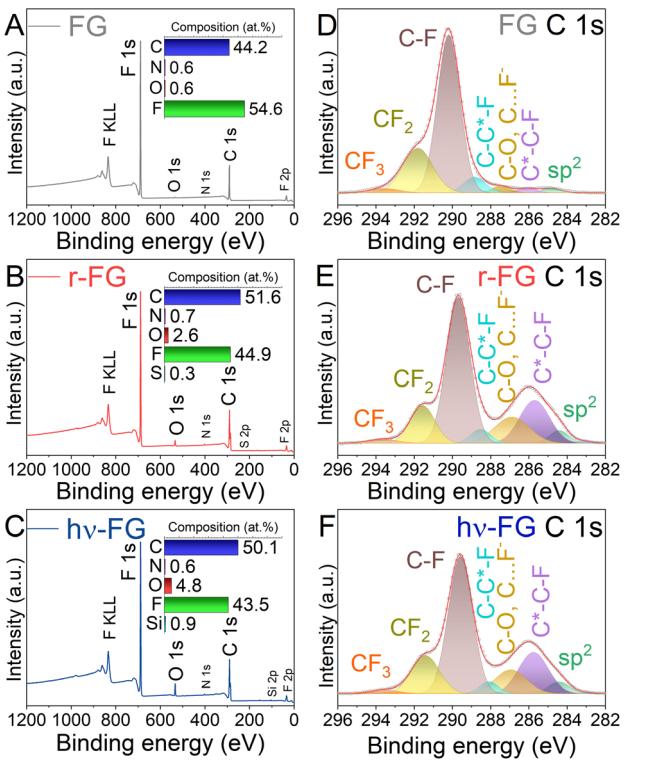

Fig. 4 XPS characterization of exfoliated FG, recovered FG (r-FG), and FG irradiated by LED 456 nm (*hν*-FG): surveys XPS spectra ((A), (B), and (C), respectively) and C 1s HR-XPS spectra ((D), (E), and (F), respectively).

of the reaction was found to be 78%, demonstrating a minor influence of suspension color on the decrease of photooxidation. Then, we turned our studies into investigating the second scenario for the high photochemical inactivation of r-FG. Considering that the inactivation of r-FG is related to the elimination of fluorine atoms from the surface of FG due to the irradiation, we assumed that intact FG layers could be exposed to our system after extended sonication of r-FG. Thus, a control experiment was conducted, using r-FG as a photochemical promoter, after 2 h of sonication. The conversion of the reaction was found to be 51%, exhibiting the low defluorination of FG as the major reason for the significant reduction of r-FG's photochemical activity. Notably, prolongation of sonication to 4 h did not result in the enhancement of r-FG's photochemical activity (conversion 49%). Overall, the diminished activity of FG after irradiation suggests that a key structural feature (defects) responsible for the rapid initial defluorination is lost after the first reaction cycle.

To elucidate the possible structural features responsible for the photoactivity, we investigated how the source material influences the performance of the FG photocatalyst. The FG used throughout this work was derived from commercial GrF supplied by Sigma Aldrich (Merck), denoted as GFS. For comparison, two additional GrF materials were examined: a lubricant-type GrF from Coreychem (GFC2L) and the product GT1F0020 from ACS material (GFA1). In contrast to GFS, both GFC2L and GFA1 exhibited significantly lower photocatalytic performance, achieving only about 40% and 22% conversion of thioanisole, respectively, under identical conditions. To understand the origin of these differences, all materials were characterized by ^{19}F solid-state NMR spectroscopy, a technique known for its sensitivity to structural defects in graphite fluorides.[63] Defective $(CF)_n$ regions manifest as downfield broadening of the main resonance line in the ^{19}F spectra, which were confirmed through spectral deconvolution.[63] Among the tested samples, GFS exhibited the highest degree of disorder (Fig. 5A), which is correlated with its superior photoactivity. Interestingly, the less active GFC2L sample exhibits a similarly high level of structural disorder (Fig. 5B), whereas GFA1, despite having comparable low activity to GFC2L, was composed predominantly of highly ordered $(CF)_n$ domains (Fig. 5C). These findings suggest that only highly defective graphite fluorides are sufficiently active for the photooxidation of sulfides at 456 nm, and that even subtle variations in structural characteristics can lead to pronounced differences in photocatalytic efficiency. Despite being a binary compound, GrF represents a structurally complex material with numerous possible defect motifs and local environments, making the identification of the specific structural features responsible for photocatalytic activity particularly challenging.

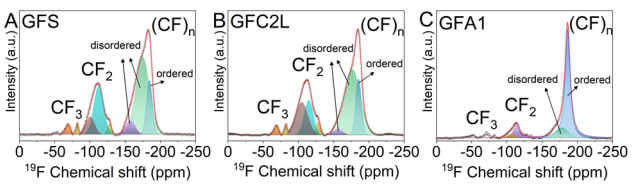

Fig. 5 NMR characterization of three different graphite fluorides as sources of FG photocatalysts; ^{19}F single-pulse TOSS MAS NMR spectra GFS (A), GFC2L (B), and GFA1 (C) graphite fluoride materials.

To reveal the nature of defects responsible for the observed photochemical activity of exfoliated FG using visible light in the spectral region of 440–470 nm, we performed time-dependent density functional theory (TDDFT) calculations for various defect motifs (see Computational details in SI). Let us recall that the optical spectral features of FG were extensively explored by some of us[35] applying the Green's function (GW) method[64,65] in combination with the Bethe–Salpeter equation (BSE) formalism within the periodic boundary conditions (PBC) framework. The PBC calculations for FG in vacuum hinted that the absorption below the optical bandgap (5.7 eV) could be attributed to midgap states stemming from radical point defects. Still, the lowest transition for a single F-vacancy recomputed here using BSE/qpGW0 was found at 3.6 eV, notably above the current active region (2.6–2.8 eV). Since strong interaction of the FG radical defects with solvents has recently been reported,[65] a similar mechanism may also play a role in the present case. Hence, we built up a series of finite-size models of FG derived from perfluoroovalene (Fig. S8 and S9 in the SI), which were shown to be sufficiently large to represent the semi-local reactivity as well as the optical properties of FG.[66,67] While the bulk solvent effects were included implicitly, a possible formation of FG-solvent charge-transfer (CT) states was assessed by including an explicit solvent molecule (MeOH or MeCN). Consistent with the PBC calculations, pristine FG and all closed-shell structures containing alkene- or benzene-like defluorinated motifs exhibit the lowest transition in the UV region well above 3.5 eV (Table S7). In addition, the mutual arrangement of frontier molecular orbitals (FMOs) of these FG models and solvent molecules (Fig. S9) implies that their absorption is not affected by intermolecular CT transitions, suggesting that perfect FG is not responsible for the observed effect. For a single F-vacancy radical defect (FG-in-C1), the vertical excitation energy (VEE) value is equal to 4.0 eV, *i.e.*, in qualitative agreement with that predicted by BSE/qpGW0. However, the HOMO of MeOH lying energetically higher than the HOMO of FG-in-C1 (Fig. S10) suggests that an intermolecular CT state with lower VEE could emerge for FG dissolved in MeOH. Indeed, the S_1 state featuring the CT character with VEE equal to 2.9 eV was found for the FG-in-C1 + MeOH model (Fig. S8). Analogous CT states with VEEs in the range of 2.7–2.9 eV were observed in the case of 3F-vacancies (Fig. S9 and S11). Notably, no such states appeared in models with MeCN due to its much lower HOMO energy (Fig. S10), which can explain the experimentally observed less efficient photoconversion of sulfides in this solvent and is in line with the measured UV-Vis spectrum of FG in MeCN (Fig. S1). The formation of the low-lying CT states predicted by the finite-size approach for radical defect structures in MeOH was also confirmed by the PBC calculations (Fig. S12 and S13). To sum up, the theoretical calculations unveiled that the formation of electron–hole separated species involved in the photooxidation of sulfides in MeOH under visible light can be rationalized by the emergence of FG-solvent CT states, due to radical point

defects (*e.g.*, F-vacancies) which are present in real FG samples (Fig. 3).[67] It is plausible to assume that the radical sites are partially passivated *via* recombination with radical species present in the reaction environment, contributing to the decreased photocatalytic activity of FG after the first reaction cycle.

Finally, to evaluate the productivity and sustainability of our protocol, a direct comparison of its catalytic results and environmental metrics with other studies was performed (see SI and Table S8). As the aerobic photooxidation of thioanisole (**1a**) to the corresponding sulfoxide **2a** has been employed in the majority of reports, the performance of this reaction was selected as a benchmark for calculating metrics in each study. The productivity rate of our protocol outperformed studies employing other carbon-based metal-free photocatalysts[50,53,55] or nanomaterials beyond carbon nanostructures,[14,68,69] since its value was found to be comparable with methods using carbon-based materials bearing organometallic units.[70,71] Importantly, in comparison with other reported studies, our protocol exhibits the strong advantage of a facile preparation of the photochemical promoter FG, as it is obtained *via* a short period of sonication (30 min) of the commercially available at low cost GrF in a low amount of solvent (0.5 mL MeOH), whereas air is the sole oxidant. To evaluate the environmental impact of our protocol, green metrics, such as Environmental Factor (*E*), Reaction Mass Efficiency (RME), and Process Mass Intensity (PMI),[72] were calculated for the photooxidation of thioansilole (**1a**). A comparison of the corresponding green metrics with several important and recent reports was conducted (Table S8). Our developed method exhibited the lowest *E* factor, which was also found to be lower than that of even catalyst-free protocols.[58] This finding demonstrated that our photochemical process produces the lowest amount of waste among the rest of the studies (Table S8). Notably, the sustainability of our method could be considered higher than that calculated, as it utilizes air as an oxidant, whereas oxygen was not taken into account in the above calculations for the studies where it was employed as a reagent.[51,52,71]

3 Conclusions

In summary, we report on the exploitation of FG's photochemical activity in the field of organic transformations for the first time. In this frame, FG was successfully employed as a photochemical promoter for the chemoselective photooxidation of organic sulfides to the corresponding sulfoxides up to high yields, under mild conditions. Based on the catalytic findings, FG acts as a metal-free photochemical promoter in the reaction, as evidenced by spectroscopic analyses. Trapping experiments revealed an oxidation mechanism involving reactive oxygen species generated by energy and/or energy transfer mechanisms from primarily photoexcited defects of FGs. Additionally, NMR studies and theoretical calculations provided mechanistic insights and rationale for observed FG's photochemical activity. Finally, the sustainability of our protocol was confirmed by evaluating green metrics, such as Environmental Factor, Reaction Mass Efficiency, and Process Mass Intensity. In this content, market availability of GrF pristine material and excellent selectivity of photooxidation without additives are significant advantages in comparison with photochemically active carbon-based benchmarks, such as carbon nitrides, carbon dots, and fullerenes. The drawback of the lack of recyclability for our protocol could be addressed by applying pulsed light irradiation in the reaction to minimize the photodecomposition of FG. All these findings render FG a promising promoter material for industrially important photooxidation processes.

Author contributions

Alessandro Tabussi: optimization, substrate scope, investigation, validation, formal analysis, data curation. Stamatis K. Serviou: optimization, investigation, validation, formal analysis, data curation. Miroslav Medved': investigation, validation, formal analysis, data curation, writing – review and editing. Vítězslav Hrubý: validation, formal analysis, writing – review and editing. Juraj Filo: formal analysis, data curation. Petr Lazar: formal analysis, data curation. Marek Cigáň: formal analysis, data curation. Demetrios D. Chronopoulos: writing – original draft, supervision, project administration, methodology. Michal Otyepka: writing – review and editing, resources. Christoforos G. Kokotos: writing – review and editing, supervision, project administration, methodology, resources, conceptualization.

Conflicts of interest

There are no conflicts to declare.

Data availability

The datasets presented in this article are openly accessible *via* Zenodo. The data supporting this article have been included as part of the supplementary information (SI). Supplementary information: optimization and mechanistic studies, experimental data and NMR traces. See DOI: https://doi.org/10.1039/d5ta09779g.

Acknowledgements

We thank Martin Petr, PhD, Jana Stráská, and Klára Čépe, PhD, for XPS measurements and TEM and AFM imaging, respectively. D. C. C. gratefully acknowledges the Hellenic Foundation for Research and Innovation (HFRI) for financial support under the "3rd Call for H. F. R. I. Research Projects to support Post-Doctoral Researchers" (Project Number: 07089). Financial support of the Scientific Grant Agency of the Slovak Republic (VEGA 1/0647/24 (M. M.) and 1/0664/25 (M. C., J. F.)) is acknowledged. M. M., V. H., P. L., and M. O. gratefully acknowledge the financial support from ERDF/ESF project TECHSCALE (No. CZ.02.01.01/00/22_008/0004587). This article has been produced with the financial support of the European Union under the REFRESH – Research Excellence for Region Sustainability and High-tech Industries project number

CZ.10.03.01/00/22_003/0000048 *via* the Operational Programme Just Transition. We acknowledge support from the Ministry of Education, Youth and Sports of the Czech Republic through the e-INFRA CZ (ID: 90254).

References

1 J. Twilton, C. Le, P. Zhang, M. H. Shaw, R. W. Evans and D. W. C. MacMillan, *Nat. Rev. Chem.*, 2017, **1**, 0052.
2 M. Silvi and P. Melchiorre, *Nature*, 2018, **554**, 41–49.
3 N.-Y. Huang, Y.-T. Zheng, D. Chen, Z.-Y. Chen, C.-Z. Huang and Q. Xu, *Chem. Soc. Rev.*, 2023, **52**, 7949–8004.
4 N. A. Romero and D. A. Nicewicz, *Chem. Rev.*, 2016, **116**, 10075–10166.
5 I. K. Sideri, E. Voutyritsa and C. G. Kokotos, *Org. Biomol. Chem.*, 2018, **16**, 4596–4614.
6 N. F. Nikitas, P. L. Gkizis and C. G. Kokotos, *Org. Biomol. Chem.*, 2021, **19**, 5237–5253.
7 P. L. Gkizis, I. Triandafillidi and C. G. Kokotos, *Chem*, 2023, **9**, 3401–3414.
8 A. Savateev and M. Antonietti, *ACS Catal.*, 2018, **8**, 9790–9808.
9 C. Rosso, G. Filippini, A. Criado, M. Melchionna, P. Fornasiero and M. Prato, *ACS Nano*, 2021, **15**, 3621–3630.
10 A. López-Magano, S. Daliran, A. R. Oveisi, R. Mas-Ballesté, A. Dhakshinamoorthy, J. Alemán, H. Garcia and R. Luque, *Adv. Mater.*, 2023, **35**, 2209475.
11 D. D. Chronopoulos, M. Otyepka and C. G. Kokotos, *ChemCatChem*, 2024, **16**, e202400042.
12 L. Zdražil, A. Cadranel, M. Medved', M. Otyepka, R. Zbořil and D. M. Guldi, *Chem*, 2024, **10**, 2700–2723.
13 I. Ghosh, J. Khamrai, A. Savateev, N. Shlapakov, M. Antonietti and B. König, *Science*, 2019, **365**, 360–366.
14 Q. Li, X. Lan, G. An, L. Ricardez-Sandoval, Z. Wang and G. Bai, *ACS Catal.*, 2020, **10**, 6664–6675.
15 J. L. Nova-Fernández, D. González-Muñoz, G. Pascual-Coca, M. Cattelan, S. Agnoli, R. Pérez-Ruiz, J. Alemán, S. Cabrera and M. Blanco, *Adv. Funct. Mater.*, 2024, **34**, 2313102.
16 P. Rana, G. Udari, B. Sridhar and S. Prakash Singh, *Chem. Eur. J.*, 2023, **29**, e202203354.
17 A. Savateev, I. Ghosh, B. König and M. Antonietti, *Angew. Chem., Int. Ed.*, 2018, **57**, 15936–15947.
18 G. Filippini, F. Longobardo, L. Forster, A. Criado, G. Di Carmine, L. Nasi, C. D'Agostino, M. Melchionna, P. Fornasiero and M. Prato, *Sci. Adv.*, 2020, **6**, eabc9923.
19 G. Grando, G. Sportelli, G. Filippini, M. Melchionna and P. Fornasiero, *Nano Trends*, 2023, **4**, 100028.
20 M. Sbacchi, M. Mamone, L. Morbiato, P. Gobbo, G. Filippini and M. Prato, *ChemCatChem*, 2023, **15**, e202300667.
21 Y. Pan, S. Wang, C. W. Kee, E. Dubuisson, Y. Yang, K. P. Loh and C.-H. Tan, *Green Chem.*, 2011, **13**, 3341–3344.
22 X. Li, J. Yu, S. Wageh, A. A. Al-Ghamdi and J. Xie, *Small*, 2016, **12**, 6640–6696.
23 G. S. Koutoulogenis, M. G. Kokotou, E. Voutyritsa, D. Limnios and C. G. Kokotos, *Org. Lett.*, 2017, **19**, 1760–1763.
24 Q. Tang, Z. Zhou and Z. Chen, *Nanoscale*, 2013, **5**, 4541–4583.
25 Y. Tong, H. Pan, W. Huang, W. Qiu, Z. Ding, C. Xu and R. Yuan, *New J. Chem.*, 2019, **43**, 8741–8745.
26 J. Cai, M. Zhang, D. Wang and Z. Li, *ACS Sustain. Chem. Eng.*, 2018, **6**, 15682–15687.
27 R. R. Nair, W. Ren, R. Jalil, I. Riaz, V. G. Kravets, L. Britnell, P. Blake, F. Schedin, A. S. Mayorov, S. Yuan, M. I. Katsnelson, H.-M. Cheng, W. Strupinski, L. G. Bulusheva, A. V. Okotrub, I. V. Grigorieva, A. N. Grigorenko, K. S. Novoselov and A. K. Geim, *Small*, 2010, **6**, 2877–2884.
28 J. T. Robinson, J. S. Burgess, C. E. Junkermeier, S. C. Badescu, T. L. Reinecke, F. K. Perkins, M. K. Zalalutdniov, J. W. Baldwin, J. C. Culbertson, P. E. Sheehan and E. S. Snow, *Nano Lett.*, 2010, **10**, 3001–3005.
29 R. Zbořil, F. Karlický, A. B. Bourlinos, T. A. Steriotis, A. K. Stubos, V. Georgakilas, K. Šafářová, D. Jančík, C. Trapalis and M. Otyepka, *Small*, 2010, **6**, 2885–2891.
30 D. D. Chronopoulos, A. Bakandritsos, M. Pykal, R. Zbořil and M. Otyepka, *Appl. Mater. Today*, 2017, **9**, 60–70.
31 X. Chen, K. Fan, Y. Liu, Y. Li, X. Liu, W. Feng and X. Wang, *Adv. Mater.*, 2022, **34**, 2101665.
32 A. Bakandritsos, M. Pykal, P. Błoński, P. Jakubec, D. D. Chronopoulos, K. Poláková, V. Georgakilas, K. Čépe, O. Tomanec, V. Ranc, A. B. Bourlinos, R. Zbořil and M. Otyepka, *ACS Nano*, 2017, **11**, 2982–2991.
33 I. Tantis, A. Bakandritsos, D. Zaoralová, M. Medveď, P. Jakubec, J. Havláková, R. Zbořil and M. Otyepka, *Adv. Funct. Mater.*, 2021, **31**, 2101326.
34 V. Šedajová, A. Bakandritsos, P. Błoński, M. Medveď, R. Langer, D. Zaoralová, J. Ugolotti, J. Dzíbelová, P. Jakubec, V. Kupka and M. Otyepka, *Energy Environ. Sci.*, 2022, **15**, 740–748.
35 V. Hrubý, L. Zdražil, J. Dzíbelová, V. Šedajová, A. Bakandritsos, P. Lazar and M. Otyepka, *Appl. Surf. Sci.*, 2022, **587**, 152839.
36 K.-J. Jeon, Z. Lee, E. Pollak, L. Moreschini, A. Bostwick, C.-M. Park, R. Mendelsberg, V. Radmilovic, R. Kostecki, T. J. Richardson and E. Rotenberg, *ACS Nano*, 2011, **5**, 1042–1046.
37 V. Mazánek, O. Jankovský, J. Luxa, D. Sedmidubský, Z. Janoušek, F. Šembera, M. Mikulics and Z. Sofer, *Nanoscale*, 2015, **7**, 13646–13655.
38 N. Watanabe, T. Nakajima and H. Touhara, *Graphite Fluorides*, Elsevier, Amsterdam, 1988.
39 N. Fukuda and T. Ikemoto, *J. Org. Chem.*, 2010, **75**, 4629–4631.
40 B. Yu, A.-H. Liu, L.-N. He, B. Li, Z.-F. Diao and Y.-N. Li, *Green Chem.*, 2012, **14**, 957–962.
41 M. Petsi and A. L. Zografos, *ACS Catal.*, 2020, **10**, 7093–7099.
42 Z.-H. Fu, H.-D. Tian, S.-F. Ni, J. S. Wright, M. Li, L.-R. Wen and L.-B. Zhang, *Green Chem.*, 2022, **24**, 4772–4777.
43 B. Di Vizio, G. Lazzari, R. Strzelczyk, G. De Crescenzo, A. Barbon, C. Garino, R. Gobetto and S. Agnoli, *Carbon*, 2025, **233**, 119856.
44 E. Skolia, P. L. Gkizis and C. G. Kokotos, *ChemPlusChem*, 2022, **87**, e202200008.

45 E. Wojaczyńska and J. Wojaczyński, *Curr. Opin. Chem. Biol.*, 2023, **76**, 102340.
46 E. Skolia, P. L. Gkizis and C. G. Kokotos, *Org. Biomol. Chem.*, 2022, **20**, 5836–5844.
47 C. K. Spyropoulou, E. Skolia, D. F. Flesariu, G. A. Zissimou, P. L. Gkizis, I. Triandafillidi, M. Athanasiou, G. Itskos, P. A. Koutentis and C. G. Kokotos, *Adv. Synth. Catal.*, 2023, **365**, 2643–2650.
48 S. K. Serviou, P. L. Gkizis, D. P. Sánchez, N. Plassais, F. Gohier, C. Cabanetos and C. G. Kokotos, *ChemSusChem*, 2024, **17**, e202400903.
49 M. V. G. Lantzanakis, C. I. Karaousta, S. K. Serviou, N. A. Stini, E. Skolia, I. Triandafillidi, A. Bota, V. P. Demertzidou and C. G. Kokotos, *Synlett*, 2025, **36**, 1514–1519.
50 P. Zhang, Y. Wang, H. Li and M. Antonietti, *Green Chem.*, 2012, **14**, 1904–1908.
51 H. Wang, S. Jiang, S. Chen, D. Li, X. Zhang, W. Shao, X. Sun, J. Xie, Z. Zhao, Q. Zhang, Y. Tian and Y. Xie, *Adv. Mater.*, 2016, **28**, 6940–6945.
52 J. Li, Y. Chen, X. Yang, S. Gao and R. Cao, *J. Catal.*, 2020, **381**, 579–589.
53 X. Chen, K. Deng, P. Zhou and Z. Zhang, *ChemSusChem*, 2018, **11**, 2444–2452.
54 A. Jozeliūnaitė, D. Valčeckas and E. Orentas, *RSC Adv.*, 2021, **11**, 4104–4111.
55 S. Rayati, A. Zamanifard, F. Nejabat and S. Hoseini, *Mol. Catal.*, 2021, **516**, 111950.
56 J. A. Tchuiteng Kouatchou, J. Farah, F. Malloggi, E. Gravel and E. Doris, *ChemCatChem*, 2024, **16**, e202400685.
57 Q. Song, W. Li, F. Shan, X. Peng, L. Wang, Z. Wang and X.-Q. Yu, *Nano Lett.*, 2024, **24**, 13895–13902.
58 E. Skolia, P. L. Gkizis, N. F. Nikitas and C. G. Kokotos, *Green Chem.*, 2022, **24**, 4108–4118.
59 E. M. Galathri, V. Hrubý, O. G. Mountanea, C. Mantzourani, D. D. Chronopoulos, M. Otyepka and C. G. Kokotos, *ChemCatChem*, 2025, **17**, e202401730.
60 C. A. Czeisler, J. K. Walsh, T. Roth, R. J. Hughes, K. P. Wright, L. Kingsbury, S. Arora, J. R. L. Schwartz, G. E. Niebler and D. F. Dinges, *N. Engl. J. Med.*, 2005, **353**, 476–486.
61 M. Ren, X. Wang, C. Dong, B. Li, Y. Liu, T. Chen, P. Wu, Z. Cheng and X. Liu, *Phys. Chem. Chem. Phys.*, 2015, **17**, 24056–24062.
62 P. Lazar, V. Hrubý, M. Petr, Z. Bad'ura, G. Zoppellaro and M. Otyepka, *Carbon*, 2025, **243**, 120567.
63 B. J. Walder and T. M. Alam, *J. Am. Chem. Soc.*, 2021, **143**, 11714–11733.
64 T. Yanai, D. P. Tew and N. C. Handy, *Chem. Phys. Lett.*, 2004, **393**, 51–57.
65 M. S. Hybertsen and S. G. Louie, *Phys. Rev. B: Condens. Matter Mater. Phys.*, 1986, **34**, 5390–5413.
66 G. Zoppellaro, M. Medved', V. Hrubý, R. Zbořil, M. Otyepka and P. Lazar, *J. Am. Chem. Soc.*, 2024, **146**, 15010–15018.
67 M. Medved', G. Zoppellaro, J. Ugolotti, D. Matochová, P. Lazar, T. Pospíšil, A. Bakandritsos, J. Tuček, R. Zbořil and M. Otyepka, *Nanoscale*, 2018, **10**, 4696–4707.
68 Z. Xie, W. Wang, X. Ke, X. Cai, X. Chen, S. Wang, W. Lin and X. Wang, *Appl. Catal. B*, 2023, **325**, 122312.
69 H. Wang, S. Chen, D. Yong, X. Zhang, S. Li, W. Shao, X. Sun, B. Pan and Y. Xie, *J. Am. Chem. Soc.*, 2017, **139**, 4737–4742.
70 D. González-Muñoz, J. Alemán, M. Blanco and S. Cabrera, *J. Catal.*, 2022, **413**, 274–283.
71 P. Blanco-Caamano, C. Navío, M. Blanco and J. Aleman, *J. Colloid Interface Sci.*, 2024, **669**, 495–505.
72 A. Quintavalla, D. Carboni and M. Lombardo, *ChemCatChem*, 2024, **16**, e202301225.